Construction and Building Materials 102 (2016) 541–551

Contents lists available at ScienceDirect

Construction and Building Materials

journal homepage: www.elsevier.com/locate/conbuildmat

Effect of confining pressure distribution on the dilation behavior in FRP-confined plain concrete columns using stone, brick and recycled aggregates

M.S.I. Choudhury, A.F.M.S. Amin *, M.M. Islam, A. Hasnat

Department of Civil Engineering, Bangladesh University of Engineering and Technology, Dhaka 1000, Bangladesh

HIGHLIGHTS

- Confined column having either large dilation or large confining pressure fails rapidly.
- Stress–strain responses are compared for confined circular and square columns.
- Significant dilation activates confinement at low stress yielding higher stiffness.
- Consequential drop in final stiffness is remarkably observed in such columns.
- Uniformity in the confining pressure distribution restrains such a phenomenon.

ARTICLE INFO

Article history:
Received 23 April 2015
Received in revised form 16 October 2015
Accepted 1 November 2015
Available online 13 November 2015

Keywords:
Fiber-reinforced polymer
Confinement
Brick aggregate concrete
Recycled stone aggregate concrete
Recycled brick aggregate concrete
Digital image correlation technique (DICT)
Dilation
Stress–strain response
Fracture behavior
Confined concrete model parameters

ABSTRACT

In a confined column, the dilation phenomenon and the geometry of the column cross-section govern the magnitude of the confining pressure and confining pressure distribution, respectively. High-definition video shows rapid post-peak failure events to occur in columns experiencing either large dilation or large confining pressure displaying a characteristically different composite action in such concretes under confinement. To investigate the origin of such a behavior, transformations in the intrinsic stiffness parameters of the fundamental stress–strain responses are critically compared between concretes having significant and insignificant dilation properties. A test database with 40 circular columns confined with fiber-reinforced polymer (FRP) subjected to uniform confining pressure distributions along with 20 unconfined (control) specimens was objectively compared with an existing symmetric test database of square columns subjected to nonuniform confining pressure distributions. Stress–strain responses of confined concrete columns with larger dilation properties revealed a significantly increased initial stiffness and markedly decreased final stiffness due to early mobilization in the FRP confinement compared to columns of stone aggregate concrete with insignificant dilation properties. The uniformity of the confining pressure distribution of circular columns has been credited with more effectively restraining the dilation-induced phenomena compared to square confined columns.

1. Introduction

The introduction of an effective confinement enhances the compression capacity of a concrete member. In practice, such confinement in a passive form is realized by installing fiber-reinforced polymer (FRP) wraps having a designed stiffness to provide the desired composite action [1–8]. An FRP wrap installed in this manner passively restricts the volumetric dilation of concrete under compression by offering a confining pressure around the perimeter of the concrete section (Fig. 1). Nevertheless, the effectiveness of the confining pressure in achieving an enhanced sectional capacity primarily depends on two factors: (i) the fundamental dilation property of the parent concrete, which determines the magnitude of the confining pressure [9,10], (ii) and the geometry of the cross section, which defines the distribution of the confining pressure (Fig. 1b and c). In this context, the primary phenomena occurring in brick and recycled aggregate concrete columns characterized by larger dilation properties in comparison to well-studied stone aggregate concrete columns necessitates a

* Corresponding author.
E-mail addresses: sichow00@gmail.com (M.S.I. Choudhury), samin@ce.buet.ac.bd (A.F.M.S. Amin), mashfiq7777@gmail.com (M.M. Islam), arifulhasnat@gmail.com (A. Hasnat).

http://dx.doi.org/10.1016/j.conbuildmat.2015.11.003
0950-0618/

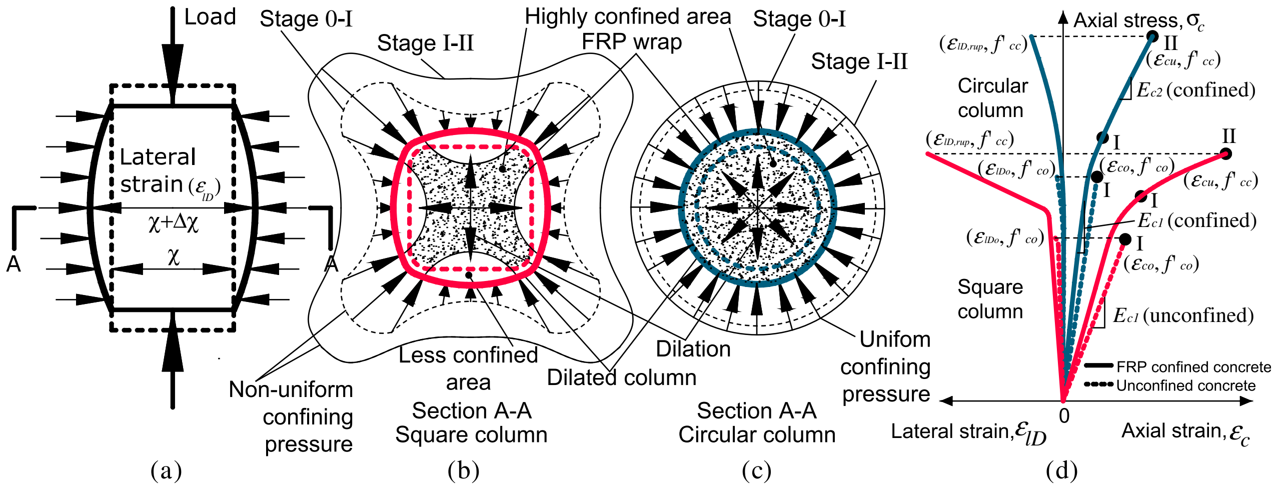

Fig. 1. Schematic representation of the dilation effect in FRP-confined circular and square columns. (a) Lateral strain caused by dilation when subjected to axial compression. Lateral strain, ε_{lD} $(=\Delta\chi/\chi)$, is a measure of the dilation effect, where χ is the initial width of the specimen and $\Delta\chi$ is the increase in width due to dilation. (b) Confining pressure distribution in a square column. (c) Confining pressure distribution in a circular column. (d) Axial stress vs. axial strain and axial stress vs. lateral strain relationships for typical unconfined and FRP-confined square and circular columns.

thorough investigation utilizing explicit experimental observations in terms of stress–strain behavior (Fig. 1d) and the fracture process.

The Poisson effect generating the volumetric dilation phenomenon in plain concrete originates from the progressive formation of micro-cracks under monotonically increasing axial stresses [11]. In plain unconfined stone aggregate concrete columns, progressive failure is characterized by three general stages [12,13]. The initiation stage is devoid of any significant cracks in the sub-microstructure and offers a linear stress–strain response, whereas the transition between the intermediate stage and the final stage is indicated by a ‘critical stress level’ that initiates a rapid increase in crack density [14]. However, concrete produced from brick and recycled aggregates are lighter in unit weights than that from stone aggregate (normal weight concrete) due to the existence of larger amount of initial micro-defects and porosities [9,10]. Thus, concretes made from brick and recycled aggregates should produce not only larger numbers of fracture planes at failure [15–17] but also larger axial strains [[18], Fig. 6 for active confinement] compared to stone aggregate concrete above their respective critical stress levels. For additional information, the recent works of González-Fonteboa et al. [19] can be referred to, where the critical stress level is found to decrease proportionately with the gradual replacement of regular stone aggregate concrete with recycled stone aggregate of the same size. Larger porosities and micro-defects producing different surface properties in the latter can explain such an observation. Although concretes composed of brick aggregate [20] and recycled brick aggregate [21] are also reported to possess larger porosities, studies that describe their fundamental fracture processes are not yet available. Recently, Amin et al. [22] discussed the roles of the characteristic surface features of recycled stone and recycled brick aggregates in providing differences in strength gain properties. However, studies that compare the intrinsic parameters, e.g., $E_{c1(\text{confined})}$, $E_{c1(\text{unconfined})}$ and $E_{c2(\text{confined})}$, of the stress–strain response of a well-studied FRP-confined stone aggregate concrete column with those of significantly dilatable brick and recycled aggregate concretes have yet to be conducted. Such a comparison can be cardinal in characterizing the composite behavior of FRP-confined concrete originating from concrete matrices with different aggregates by well supplementing the large established test databases for stone aggregate concrete columns with the objective of rationalizing existing confined concrete models [[18,23–27] and references cites therein] from a more general perspective.

Furthermore, any significant variation in the fracture behavior in terms of the number of fracture planes and the size of fractured particles of concretes originating from within the concrete matrices should incorporate differences in the nonuniformity of the confining pressure due to the developed heterogeneity and dispersion of fractured particles. These are known to be potential factors in generating stress concentrations that are much higher than the average confinement pressure by pricking the FRP wrap, leading to a very rapid explosive failure process [4,6,28]. The failure scenarios between circular and noncircular FRP-confined columns having uniform (Fig. 1c) and non-uniform (Fig. 1b) confining pressure distributions will be different because the latter allows for larger dilation in segments of the perimeter where the confining pressure is low. However, in contrast to experiments with unconfined concrete, the progressive development of cracking phenomena is hardly visible in FRP confined concrete before a rupture occurs in the wrap. The unavailability of such a vital experimental observation requires designers to adopt a very strict so-called conservative approach in assigning strength enhancement limits (Section 1.3.1 and Section 9.2 of ACI 440.2R [8]) based on the minimal experimental information available for such a fracture process.

With these backgrounds, the current study attempted to gather fundamental experimental information on the progressive mobilization of confinement due to the dilation phenomenon and to study its effect on post-peak failure events. The axial stress, axial strain and dilation histories of the test pieces at the exact failure location due to the axial load were measured using the digital image correlation technique (DICT). To passively identify the effects of intrinsic fracture processes occurring in concretes having larger dilation properties in generating the composite action, the stress–strain responses for FRP-confined circular and square columns in terms of $E_{c1(\text{confined})}$ and $E_{c2(\text{confined})}$ (Fig. 1d) are compared for concretes having insignificant (stone aggregate concrete) and significant (brick and recycled aggregate concretes) dilation properties. The responses for unconfined specimens with corresponding geometries are compared for circular and square cross sections. The post-peak failure events are compared in terms of the time required to reach complete failure after sustaining the peak load. Finally, the confinement model coefficients estimated for circular concrete columns composed of stone, brick and recycled aggregates are compared with those obtained for square concrete columns composed of the same aggregates based on the results published in a recent study [9].

2. Experiments

This study reports on an experimental investigation in which the stress–strain and post-peak failure processes of a group of FRP-confined concrete columns were thoroughly investigated and compared to unconfined columns with DICT measurements at the failure location. The fundamental dilation property of the parent concrete and the confining pressure distribution were used as experimental variables to investigate the confinement mechanism in concretes having significant dilation properties up to and beyond the ultimate load. Carbon-FRP (CFRP) and glass-FRP (GFRP) were used to confine the columns at different magnitudes. The source of the coarse aggregates, specimen preparation procedures, properties of the FRP wraps, FRP application procedures, testing and data acquisition procedures were consistent for each tested specimen.

Fig. 2 shows close-up photographs of the coarse aggregates from crushed burnt clay bricks, crushed stones and aggregates recycled from crushed old brick and stone aggregate concretes. Table 1 provides specimen descriptions and the sample nomenclature used throughout this paper. Detailed descriptions of the material properties,

Table 1
Specimen description and sample ID.
Partially reprinted from M.M. Islam, M.S.I. Choudhury, A.F.M.S. Amin, Dilation effects in FRP-confined square concrete columns using stone, brick, and recycled coarse aggregates, J. Compos. Constr. ASCE (2015), http://dx.doi.org/10.1061/(ASCE)CC.1943-5614.0000574. 04015017, with permission from ASCE.

Shape	Aggregate type	Specimen ID	Confinement type	No. of specimens
Circular columns	Brick (B)	BCCON	Unconfined	5
		BCCFRP	CFRP wrap	5
		BCGFRP	GFRP wrap	5
	Stone (S)	SCCON	Unconfined	5
		SCCFRP	CFRP wrap	5
		SCGFRP	GFRP wrap	5
	Recycled brick (RB)	RBCCON	Unconfined	5
		RBCCFRP	CFRP wrap	5
		RBCGFRP	GFRP wrap	5
	Recycled stone (RS)	RSCCON	Unconfined	5
		RSCCFRP	CFRP wrap	5
		RSCGFRP	GFRP wrap	5
Square columns after Islam et al. [9]	Brick (B)	BSCON	Unconfined	5
		BSCFRP	CFRP wrap	5
		BSGFRP	GFRP wrap	5
	Stone (S)	SSCON	Unconfined	5
		SSCFRP	CFRP wrap	5
		SSGFRP	GFRP wrap	5
	Recycled brick (RB)	RBSCON	Unconfined	5
		RBSCFRP	CFRP wrap	5
		RBSGFRP	GFRP wrap	5
	Recycled stone (RS)	RSSCON	Unconfined	5
		RSSCFRP	CFRP wrap	5
		RSSGFRP	GFRP wrap	5

Notes: For the five specimens mentioned for each confinement type, the specimen sizes are as follows. Circular columns: Size 1 (2 Nos.): 100 mm in diameter, 200 mm in height; Size 2 (2 Nos.): 150 mm in diameter, 300 mm in height, Size 3 (1 No.): 200 mm in diameter, 400 mm in height. Square columns – Size 4 (2 Nos.): 100 × 100 × 200 mm; Size 5 (2 Nos.): 150 × 150 × 300 mm; Size 6 (1 No.): 200 × 200 × 400 mm.

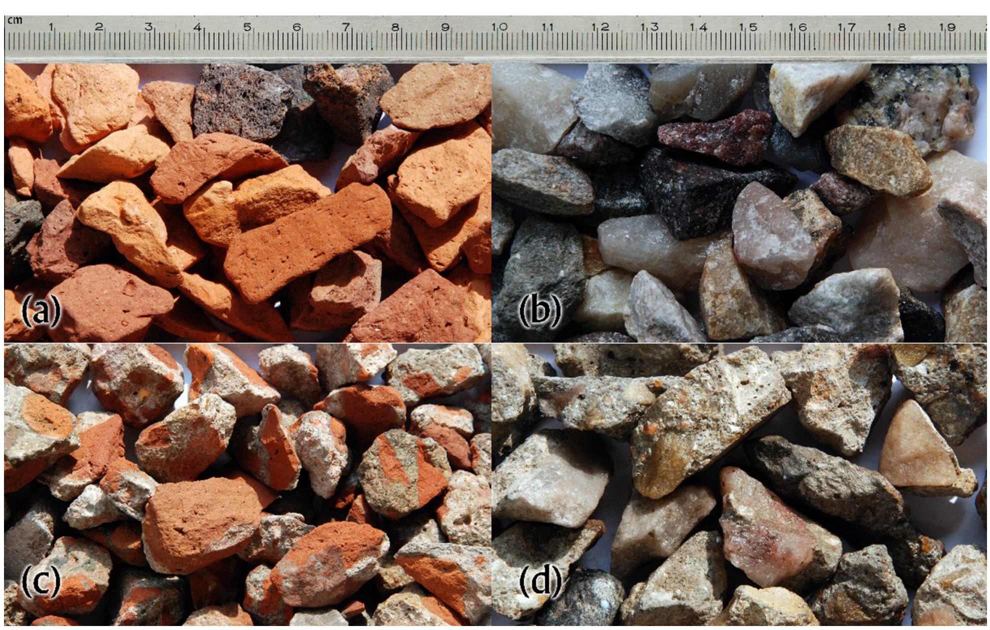

Fig. 2. Types of coarse aggregates used in the research. (a) Brick aggregate, (b) stone aggregate, (c) recycled brick aggregate, and (d) recycled stone aggregate. The aggregates were 12–19 mm in size. Partially reprinted from M.M. Islam, M.S.I. Choudhury, A.F.M.S. Amin, Dilation effects in FRP-confined square concrete columns using stone, brick, and recycled coarse aggregates, J. Compos. Constr. ASCE (2015), http://dx.doi.org/10.1061/(ASCE)CC.1943-5614.0000574. 04015017, with permission from ASCE. Images by A.F.M.S. Amin.

Table 2
Experimental results of circular column specimens.

CA type	Specimen ID	Size	ε_{co}	ε_{cu}	ε_{lD}	f'_{co} (MPa)	f'_{cc} (MPa)
Brick	BCCON	1	0.0014	–	0.0047	29.75	–
		1	0.0013	–	0.0047	29.90	–
		2	0.0008	–	0.0027	23.47	–
		2	0.0008	–	0.0107	25.62	–
		3	0.0006	–	0.0076	23.93	–
	BCCFRP	1	–	0.0021	0.0090	–	39.81
		1	–	0.0023	0.0182	–	46.77
		2	–	0.0020	0.0080	–	38.90
		2	–	0.0019	0.0080	–	37.73
		3	–	0.0009	0.0073	–	33.03
	BCGFRP	1	–	0.0031	0.0213	–	54.21
		1	–	0.0039	0.0180	–	47.80
		2	–	0.0029	0.0103	–	44.70
		2	–	0.0025	0.0159	–	42.23
		3	–	0.0019	0.0098	–	37.80
Stone	SCCON	1	0.0011	–	0.0025	29.16	–
		1	0.0013	–	0.0053	28.86	–
		2	0.0007	–	0.0013	29.39	–
		2	0.0007	–	0.0108	35.21	–
		3	0.0006	–	0.0050	32.59	–
	SCCFRP	1	–	0.0025	0.0077	–	55.94
		1	–	0.0025	0.0135	–	55.05
		2	–	0.0017	0.0050	–	43.87
		2	–	0.0018	0.0080	–	47.33
		3	–	0.0013	0.0100	–	38.98
	SCGFRP	1	–	0.0035	0.0093	–	67.37
		1	–	0.0022	0.0179	–	54.21
		2	–	0.0022	0.0077	–	56.32
		2	–	0.0020	0.0077	–	56.28
		3	–	0.0016	0.0099	–	47.89
Recycled brick	RBCCON	1	0.0013	–	0.0116	24.31	–
		1	0.0016	–	0.0110	26.84	–
		2	0.0009	–	0.0023	32.58	–
		2	0.0009	–	0.0046	29.88	–
		3	0.0008	–	0.0055	28.16	–
	RBCCFRP	1	–	0.0031	0.0153	–	49.08
		1	–	0.0027	0.0153	–	49.43
		2	–	0.0020	0.0190	–	43.22
		2	–	0.0025	0.0090	–	42.56
		3	–	0.0013	0.0023	–	33.89
	RBCGFRP	1	–	0.0045	0.0150	–	53.23
		1	–	0.0046	0.0110	–	53.31
		2	–	0.0025	0.0113	–	47.60
		2	–	0.0029	0.0138	–	47.99
		3	–	0.0012	0.0099	–	34.88
Recycled stone	RSCCON	1	0.0013	–	0.0076	22.88	–
		1	0.0013	–	0.0078	27.63	–
		2	0.0009	–	0.0027	22.44	–
		2	0.0011	–	0.0025	20.18	–
		3	0.0006	–	0.0050	26.10	–
	RSCCFRP	1	–	0.0030	0.0153	–	51.36
		1	–	0.0026	0.0153	–	50.68
		2	–	0.0020	0.0080	–	39.65
		2	–	0.0019	0.0134	–	45.08
		3	–	0.0013	0.0123	–	38.33
	RSCGFRP	1	–	0.0033	0.0113	–	61.18
		1	–	0.0044	0.0188	–	60.13
		2	–	0.0028	0.0353	–	48.55
		2	–	0.0026	0.0353	–	47.00
		3	–	0.0015	0.0123	–	37.19

Notes: Circular columns: Size 1 (2 nos): 100 mm in diameter, 200 mm in height; Size 2 (2 nos): 150 mm in diameter, 300 mm in height, Size 3 (1 No.): 200 mm in diameter, 400 mm in height.

specimen preparation and testing procedures have already been reported elsewhere [9,29,30] and are omitted here for the sake of brevity. Table 2 provides the measured ε_{co}, ε_{cu}, ε_{lD}, f'_{co} and f'_{cc} values of the circular specimens. The unconfined compressive strengths of the concrete specimens ranged between 20 and 35 MPa, with an average strength of 27 MPa. Of the experimental data set findings, only typical test results are used in the following discussion and conclusions.

Fig. 3 illustrates two groups of unconfined (Fig. 3a) and FRP-confined specimens (Fig. 3b) of different sizes. Customized molds were used to ensure uniformity in size and shape, as per Table 1. The corners of all square columns were uniformly rounded to a radius of 25 mm using customized molds to reduce stress concentration. All specimens were tested under uniaxial compression at a constant stress rate of 0.21 MPa/s up to the ultimate (peak) load. High-definition video for each of the tests was recorded until the completion of the failure process. Axial stress (σ_c), axial strain (ε_c) and lateral strain (ε_{lD}) data were recovered from load cell data and were well correlated with the corresponding video footage for the plotting of the results.

3. Results and discussion

3.1. Fracture process of confined specimens

At the ultimate state, failure of the confined column is signified by the loss of confining pressure due to failure of the FRP wrap [4,28]. The number of failure planes generated up to the peak load determines the rupture process of the FRP wrap that was providing the confinement [14–19]. The rupture of FRP confinement in the final moments after experiencing the peak load should ideally be governed by not only the ultimate hoop strain but also the fragments of concrete being confined by the FRP wrap, as postulated by Abdelrahman and El-Hacha [31].

Fig. 4 shows the progressive failure of a circular stone aggregate concrete column confined with CFRP. A typical failure of a brick aggregate concrete column with the same geometry and confinement is illustrated in Fig. 5. The attached video clip (Video Clip 1a) shows the confined column during the last six seconds of the test. The complete test is shown at a lower resolution in Video Clip 1b. After experiencing the peak load, the failure process of the stone aggregate concrete column was completed in 3.07 s, whereas the failure process of the brick aggregate concrete column was completed in only 0.82 s. Furthermore, at the very beginning of the failure of the stone aggregate concrete column, no concrete spalling is visible (Fig. 4b). In contrast, the failure process of the brick aggregate concrete column (Fig. 5 and Video Clip 2) involved a complete disintegration of concrete immediately upon the loss of confinement.

Furthermore, the comparison of the data for columns with nonuniform pressure distributions shows that the post-peak failure process for the smallest square recycled stone aggregate concrete column (Fig. 6 and Video Clip 3) was completed in 1.93 s, and the post-peak failure process of the largest square concrete column (Fig. 7 and Video Clip 4) was completed in 2.23 s. The failure of a large specimen involves not only the loss of confinement due to the failure of the corner zone but also events in the less confined sides of the square column.

The plots presented in Fig. 8 comprehensively compare the failure times for different specimen sizes and confining pressure distributions. The post-peak failure process for square columns with nonuniform confining pressure distributions was generally longer than for the circular columns of the same aggregate type (Fig. 8a–d). This pattern may be due to the redistribution of confining pressure after Stage I (Fig. 1b), therein producing larger dilation in the less confined sides. This proposition will be further investigated in Section 3.3 by scrutinizing the intrinsic parameters of the stress–strain responses.

Nevertheless, the failure time of the stone aggregate concrete columns was generally longer than that of the columns composed of aggregates with significant dilation properties (Fig. 8a and b). However, when comparing columns of different sizes, square columns composed of stone aggregate concrete with longer sides but the same corner radius were found to require more time to fail after the peak load (Fig. 8b and d). The failure process of large columns composed of brick and recycled aggregate concrete (with greater dilation properties) required less time compared to the columns composed of stone aggregate concrete. The images in Figs. 6 and 7 show the abrupt failures due to dilation (see also the related video clips). Interestingly, the failure times of the smaller square and circular columns (Fig. 8c and d) were similar for all aggregate

(a) (b)

Fig. 3. Columns with different geometries and coarse aggregate types prepared for testing. (a) Unconfined columns before FRP wrap installation. (b) Columns of four aggregate types confined with CFRP wrap.

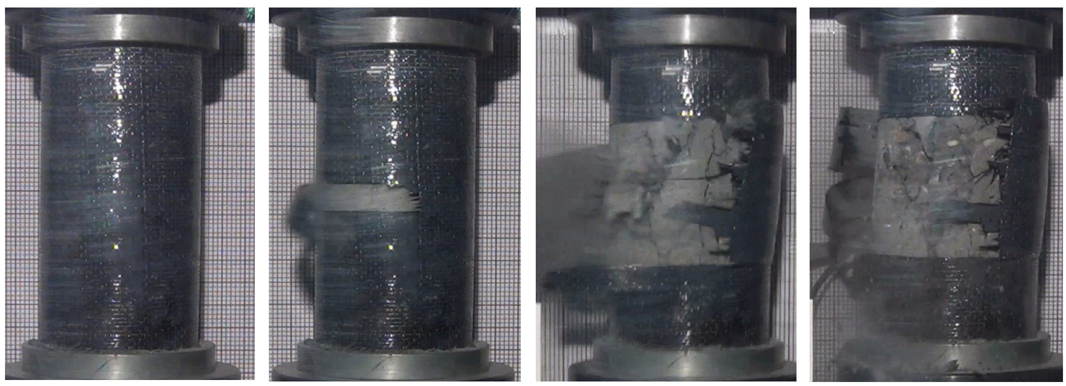

(a) (b) (c) (d)

Fig. 4. Progressive failure of a stone aggregate concrete CFRP column (150 mm in diameter, 300 mm in height) under axial compression captured using high-definition video. Locations of the still image frames in the HD footage in the vicinity of Stage II: (a) 3:48 min: 52/60 frame, (b) 3:51 min: 35/60 frame, (c) 3:51 min: 39/60 frame, and (d) 3:51 min: 56/60 frame. This timeline corresponds to Video Clip 1b. Images by A.F.M.S. Amin.

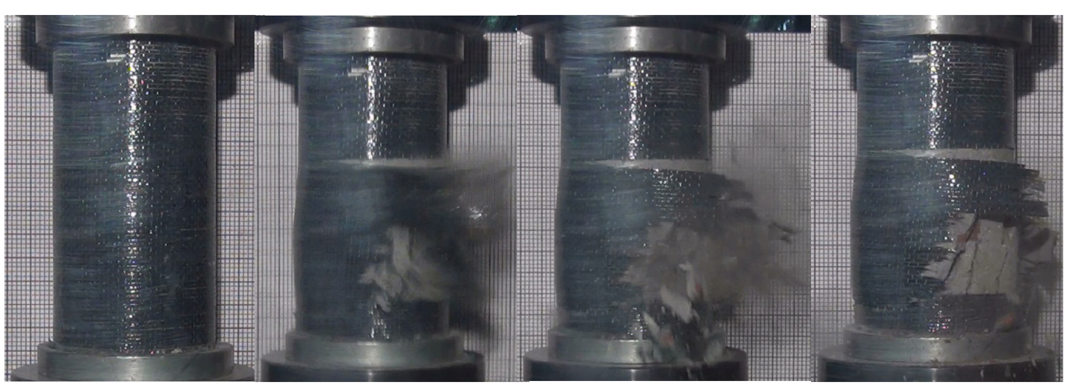

(a) (b) (c) (d)

Fig. 5. Progressive failure of a brick aggregate concrete CFRP-confined column (150 mm in diameter, 300 mm in height) under axial compression captured using high-definition video. Large dilation is visible in panel (b). Locations of the still image frames in the HD footage in the vicinity of Stage II: (a) 3:05 min: 11/60 frame, (b) 3:05 min: 42/60 frame, (c) 3:05 min: 46/60 frame, and (d) 3:06 min: 00/60 frame. This timeline corresponds to Video Clip 2b. Images by A.F.M.S. Amin.

types. Taken together, the observations described here indicate the necessity of considering more stringent safety factors for issuing early warnings prior to a complete collapse, particularly in cases where the concretes have a large dilation property and where the confining pressures are either high or uniform. In Sections 3.2 and 3.3, the observations on post-peak fracture processes are correlated with the dilation effect on the transformation of the stress–strain responses.

3.2. Dilation effect in concretes from different aggregates

Fig. 9 presents a comparison of the data sets obtained via strain measurements at the locations of failure due to axial compression in circular and square concrete columns composed of significantly dilatable (brick and recycled aggregate) and less dilatable (stone aggregate) concrete. The unconfined columns reached Stage I with an initial stiffness of $E_{c1(\text{unconfined})}$ between stress levels of

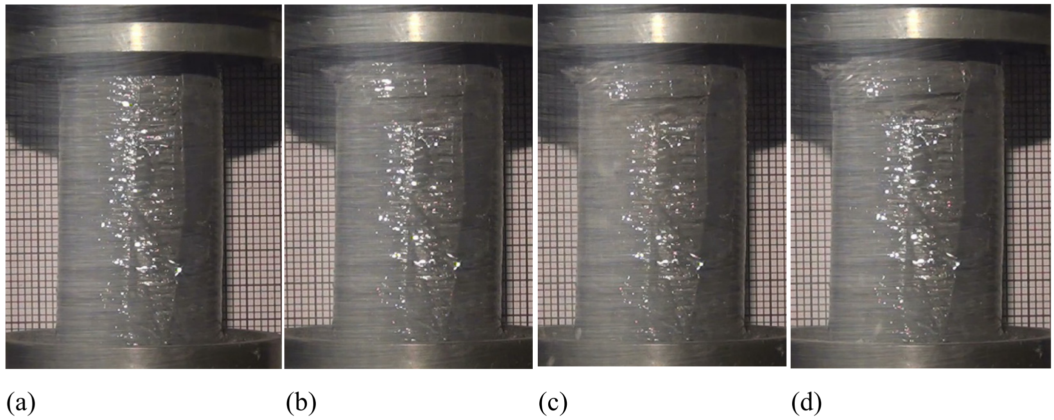

Fig. 6. Progressive failure of a recycled stone aggregate concrete GFRP column (100 × 100 × 200 mm) under axial compression captured on high-definition video. Locations of the still image frames in the HD footage in the vicinity of Stage II: (a) 2:41 min: 04/60 frame, (b) 2:42 min: 54/60 frame, (c) 2:43 min: 04/60 frame, and (d) 2:44 min: 00/60 frame. This timeline corresponds to Video Clip 3b. Images by A.F.M.S. Amin.

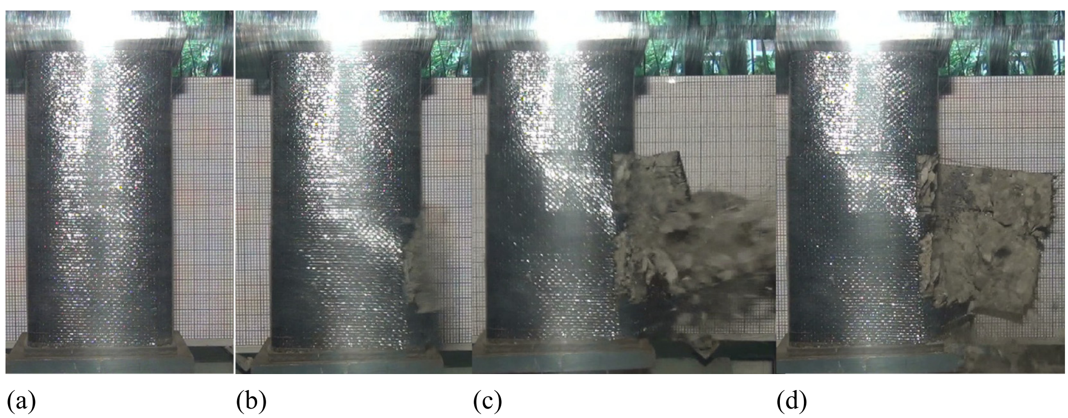

Fig. 7. Progressive failure of a recycled stone aggregate concrete CFRP-confined column (200 × 200 × 400 mm) under axial compression captured on high-definition video. Large dilation is visible in panel (b). Locations of the captured still image frames in the HD footage in the vicinity of Stage II: (a) 2:38 min: 09/60 frame, (b) 2:30 min: 05/60 frame, (c) 2:30 min: 08/60 frame, and (d) 2:30 min: 23/60 frame. This timeline corresponds to Video Clip 4b. Images by A.F.M.S. Amin.

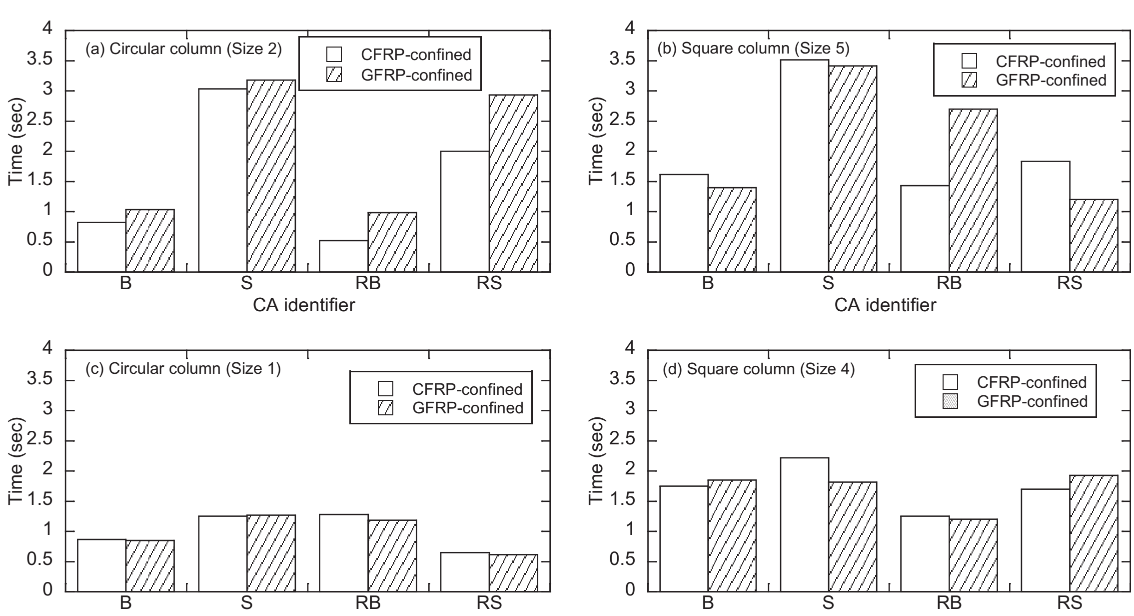

Fig. 8. Post-peak failure times recorded for different specimens using DICT. Initiation of the failure process was identified by localized visual movement of FRP confinement. The time measurement starts when the failure process initiates and ends when the fracture process is complete.

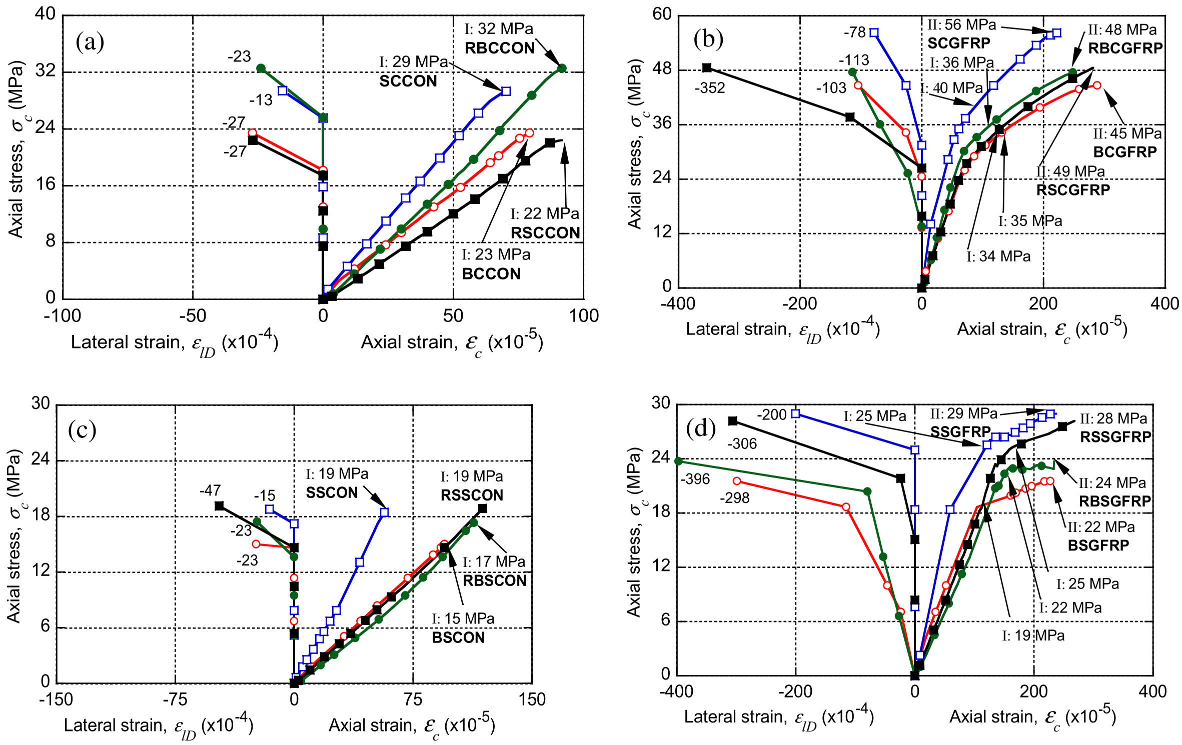

Fig. 9. Dilation effects in the circular and square columns. (a) Unconfined circular column (Size 2: 150 mm in diameter, 300 mm in height) results for stone (SCCON), brick (BCCON), recycled stone (RSCCON) and recycled brick (RBCCON) aggregates. (b) Glass-FRP (GFRP)-confined circular column (Size 2: 150 mm in diameter, 300 mm in height) results for stone (SCGFRP), brick (BCGFRP), recycled stone (RSCGFRP) and recycled brick (RBCGFRP) aggregates. (c) Unconfined square column (Size 5: 150 × 150 × 300 mm; corner radius: 25 mm) results for stone (SSCON), brick (BSCON), recycled stone (RSSCON) and recycled brick (RBSCON) aggregates. (d) GFRP-confined square column (Size 5: 150 × 150 × 300 mm; corner radius: 25 mm) results for stone (SSGFRP), brick (BSGFRP), recycled stone (RSSGFRP) and recycled brick (RBSGFRP) aggregates (data from Islam et al. [9] for Fig. 9(c) and 9(d)).

20–35 MPa with an average stress of approximately 27 MPa. The responses from all columns contain the E_{c2} branch that was observed in the confined columns. The ultimate strains ε_{cu} and ε_{lD} were also found to be distinctly smaller for the stone aggregate concrete than for the brick or recycled aggregate concretes (Table 2). In general, due to the effect of dilation, unconfined and confined columns composed of stone aggregate concrete exhibited distinctly stiffer behavior with respect to σ_c vs. ε_c and σ_c vs. ε_{lD} than did columns composed of brick and recycled aggregate concretes. The observation of such a phenomenon necessitates a careful examination of the stress–strain responses and post-peak events through comparisons.

3.3. Effect of confining pressure distribution on stress–strain behavior

The axial stiffness of a column with FRP confinement, based on the extensive test database of stone aggregate concrete, is assumed to be ideally represented by the stiffness of the parent (unconfined) concrete up to f'_{co} (Fig. 1, Stage 0–I, Shahawy et al. [4], Youssef et al. [32], Teng et al. [33]), beyond which a decrease in stiffness occurs due to the progressive failure of the core concrete (Stage I–II). The sufficiency of the employed confinement governs the increasing or decreasing stiffness of the second branch [6–8,27]; also Fig. 6 in [25]. The observations of Sfer et al. 2002 [34] from tri-axial tests on plain concrete under active confinement are analogous to this concept.

In this context, the stress–strain behaviors of the circular and square columns composed of the four aggregate types are further compared in Fig. 10. The responses of corresponding unconfined columns are also plotted for comparison. The stone aggregate concrete column experienced a higher ultimate load (Fig. 10b), a lower axial strain (ε_{cu}) and a lower lateral strain than did the concrete columns from brick and recycled aggregates (Fig. 10a, c and d). A thorough comparison of the specimens vividly demonstrates several characteristic differences between the square and circular columns under both unconfined and confined states. These differences are clearly due to the intrinsic effects related to the uniformity and nonuniformity of the stress distributions of the critical cross section at the specimen height where the failure occurred. Compared to the unconfined columns, the increase in the initial stiffness, $E_{c1(\mathrm{confined})}$, was smaller for the square columns than for the circular columns. A comparison of the data for the different aggregates shows that the stiffness increase appeared to be greater for concrete columns using aggregates having significant dilation properties. This is in conformity with the concept of the initiation of the progressive development of microcracks in concretes from brick and recycled aggregates at a lower critical stress level than that for stone aggregate concrete [11–19].

Furthermore, the response producing the final stiffness, $E_{c2(\mathrm{confined})}$, of the square columns sustained for a smaller strain between Stage I and Stage II than for the circular columns. This difference was more pronounced in the circular columns composed of concrete made from brick and recycled aggregates with larger dilation properties. Additionally, the $E_{c2(\mathrm{confined})}$ values for the square columns were markedly lower than those measured for the circular columns.

A comparison of the $E_{c1(confined)}/E_{c1(unconfined)}$ and E_{c2} ratios for the different aggregates is presented in Tables 3 and 4. The $E_{c1(confined)}/E_{c1(unconfined)}$ ratio was greater for brick and recycled aggregates than for the stone aggregate, and the difference was particularly pronounced for the square columns. The distinct increase in stiffness as observed in specimens having significant dilation properties before reaching Stage-I exhibits a direct relation with the fracture process narrated in Section 3.1, where the failure process

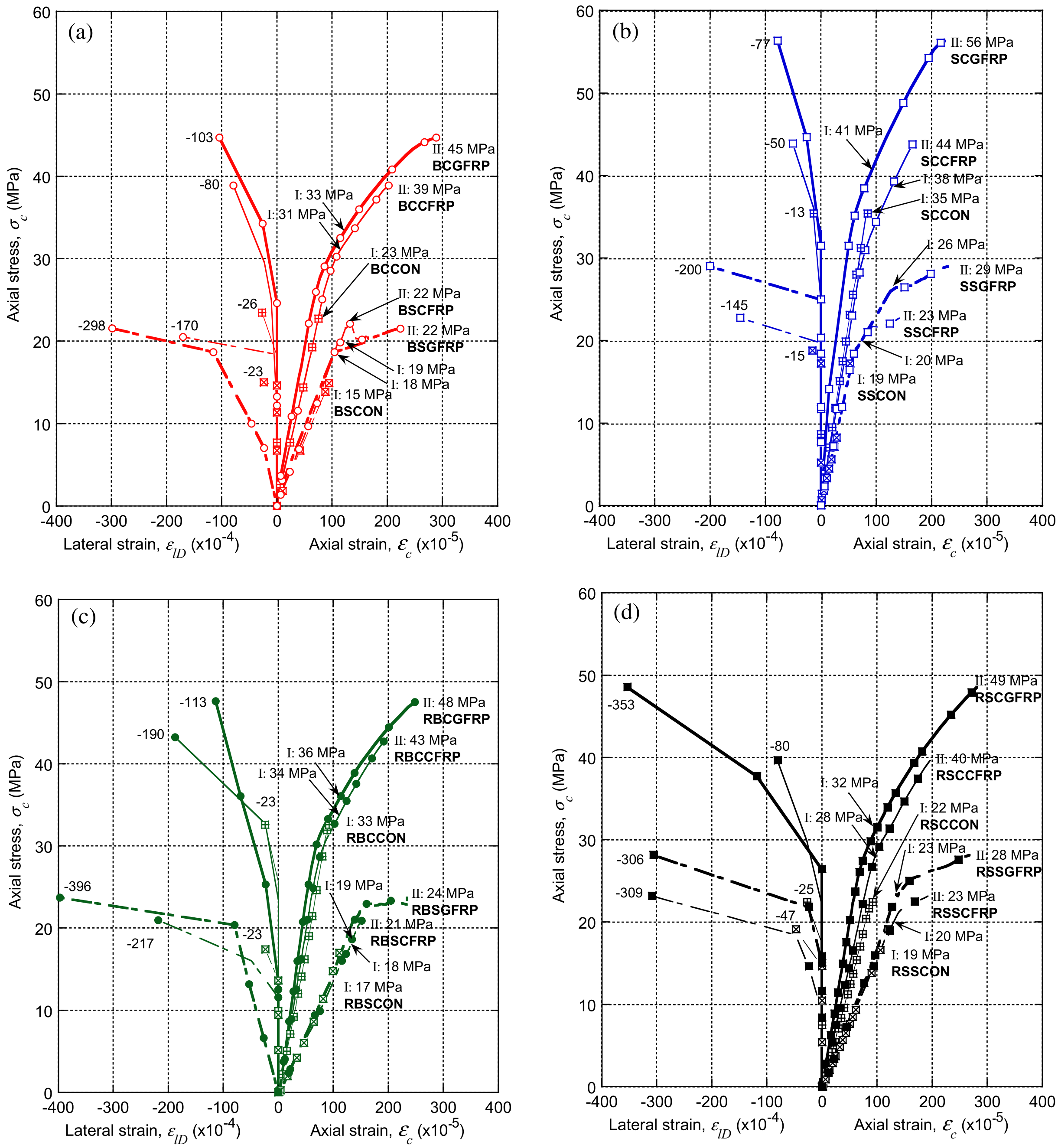

Fig. 10. Axial and lateral stress–strain responses of concrete columns with different aggregates for Size 2 (150 mm in diameter, 300 mm in height) and Size 5 (150 × 150 × 300 mm) specimens. (a) Brick aggregate concrete, (b) stone aggregate concrete, (c) recycled brick aggregate concrete, and (d) recycled stone aggregate concrete (data from Islam et al. [9] for the responses of square columns).

of the stone aggregate concrete column required more time than did that of the concrete columns with significant dilation properties (3.07 s vs. 0.82 s for stone and brick aggregate concrete columns, respectively; Section 3.1). Furthermore, a complete disintegration of concrete was noted for the brick aggregate concrete column (Fig. 5 and Video Clip 2). An early mobilization of FRP confinement through the internal disintegration of concretes with large dilation properties must be responsible for such a phenomenon.

In contrast, the E_{c2} values for the brick and recycled aggregate concretes were distinctly lower than the E_{c2} values for the corresponding stone aggregate concrete specimens. This decrease was more prominent for the circular columns than for the square columns. Nevertheless, these observations clearly indicate an early confinement mobilization in concrete columns with significantly dilatable aggregates, which activate the FRP confinement at a lower axial strain, thereby increasing the initial stiffness values. After Stage I, disintegration of the concrete matrix in brick and recycled aggregate concrete columns was substantial compared to the stone aggregate columns. This disintegration led to a significant reduction in the E_{c2} values for the brick and recycled aggregate concrete columns with respect to the values for the stone aggregate concrete columns (Table 3). The larger decrease in E_{c2}values as observed for the square columns than for the circular columns with uniform confining pressure distributions (Fig. 1c) exhibits a strong correlation with the fracture process observed in Section 3.1 (Figs. 6–8).

Table 3
$E_{c1(confined)}/E_{c1(unconfined)}$ values for different specimens.

CA type	Confinement type	$E_{c1(confined)}/E_{c1(unconfined)}$					
		Circular column			Square column		
		Size 1	Size 2	Size 3	Size 4	Size 5	Size 6
B	CFRP confined	1.21	1.00	1.00	1.77	1.08	1.26
	GFRP confined	1.36	1.28	1.00	1.89	1.21	1.00
S	CFRP confined	1.00	1.00	1.00	1.44	1.00	1.00
	GFRP confined	1.65	1.17	1.21	1.66	1.00	0.97
RB	CFRP confined	1.15	1.15	1.00	1.31	1.00	1.16
	GFRP confined	1.04	1.16	0.99	1.55	1.16	1.16
RS	CFRP confined	1.44	1.22	1.18	1.42	1.01	1.22
	GFRP confined	1.72	1.57	1.18	1.43	1.10	1.00

Notes: Circular columns - Size 1: 100 mm in diameter, 200 mm in height; Size 2: 150 mm in diameter, 300 mm in height, Size 3: 200 mm in diameter, 400 mm in height. Square columns – Size 4: 100 × 100 × 200 mm; Size 5: 150 × 150 × 300 mm; Size 6: 200 × 200 × 400 mm.

Table 4
Relative change in E_{c2} values for confined columns with B, RB and RS found by normalizing the values in terms of S.

CA type	Confinement type	E_{c2} (MPa), normalized w.r.t. respective specimen of stone aggregate concrete, S					
		Circular column			Square column		
		Size 1	Size 2	Size 3	Size 4	Size 5	Size 6
B	CFRP confined	0.56	0.61	0.98	–	1.10	–
	GFRP confined	0.77	0.73	0.87	0.79	0.95	1.05
S	CFRP confined	1.00	1.00	1.00	1.00	1.00	1.00
	GFRP confined	1.00	1.00	1.00	1.00	1.00	1.00
RB	CFRP confined	0.60	0.70	0.86	1.23	0.98	0.51
	GFRP confined	0.54	0.75	1.06	0.69	1.05	1.19
RS	CFRP confined	0.74	0.68	0.68	1.43	0.67	0.82
	GFRP confined	0.81	0.76	0.81	0.76	1.10	0.95

The ultimate state, the basis for design guidance ACI 440.2R [8], is compared by constructing parity plots for square and circular specimens in Fig. 11. The plots generally show distinctly larger f'_{cc} values for circular columns (Fig. 11a). Under a similar ultimate axial strain, ε_{cu} (Fig. 11b), the square columns underwent greater dilation, ε_{lD}, than did the circular columns (Fig. 11c). Fig. 11a shows that a smaller increase in axial capacity f'_{cc} was associated with the change in confining pressure distribution (square to circular) for the columns composed of concretes having significant dilation properties. Fig. 11c further supports this observation: distinctly larger dilation values were observed for square columns compared to circular columns, particularly for the significantly dilatable concretes. Furthermore, the f'_{cc} values for square columns fell within a narrow range because the corner radius (the most important governing parameter for such columns) was equal (25 mm) for all the specimens. This constant value resulted in similar amounts of confinement. However, the f'_{cc} values for the circular columns fell in a wide range due to variations in diameter, which resulted in a wide variety of confining pressure magnitudes (see also Section 3.4).

3.4. Effect on confinement design

The confinement model coefficients, e.g., k_1k_{s1} and k_2k_{s2} in Eqs. (1)–(3), which are derived to represent the ultimate condition (Stage II, Fig. 1d), dictate the design of the FRP confinement [8]:

$$\frac{f'_{cc}}{f'_{co}} = 1 + k_1k_{s1}\frac{f_{lD}}{f'_{co}} \quad (1)$$

$$\frac{\varepsilon_{cu}}{\varepsilon_{co}} = 1 + k_2k_{s2}\frac{f_{lD}}{f'_{co}} \quad (2)$$

$$f_{lD} = \frac{2E_{frp}\varepsilon_{lD}t_{frp}}{D} \quad (3)$$

where k_1 is the confinement effectiveness coefficient; k_2 is the strain enhancement coefficient; k_{s1} and k_{s2} are factors governed by the specimen's shape and therefore determine the confining pressure distribution that controls f'_{cc}; E_{frp} and t_{frp} are the modulus of elasticity and the FRP wrap thickness, respectively; f_{lD} is the confining pressure due to the FRP wrap when the concrete fails by rupture due to hoop tensile stresses; and D is the equivalent column diameter. The design parameters, (k_1k_{s1} and k_2k_{s2}, in Eqs. (1)–(3)) are derived in Fig. 12 for circular columns. The relationships between the confinement models (Eqs. (1) and (2)) for the square columns [9] are also plotted for comparison. The behaviors of circular and square columns clearly differ. The determined k_1k_{s1} parameter values were very similar for circular columns composed of each of the four aggregate types but were also very similar to the suggested values in ACI 440.2R [8]. For circular columns, no significant divergence between the values for less dilatable (stone aggregate concrete) and largely dilatable (brick and recycled aggregate) concretes was found. In contrast, square columns exhibited [9] considerably larger differences in value between the aggregate types (1.42 for brick aggregate, 1.55 for recycled brick aggregate, 0.89 for recycled stone aggregate concretes and 2.35 for stone aggregate concrete).

In the case of the parameters k_2k_{s2} , the divergence in values between less dilatable and significantly dilatable concretes is weaker for the circular columns than for the square columns (i.e., 1.32 for brick aggregate, 1.00 for recycled brick aggregate, 1.20 for recycled stone aggregate concretes and 6.90 for stone aggregate concrete). The ACI 440.2R [8] suggested values are also somewhat larger than those estimated from the stone aggregate concrete column experimental data, as previously noted and discussed [9] in

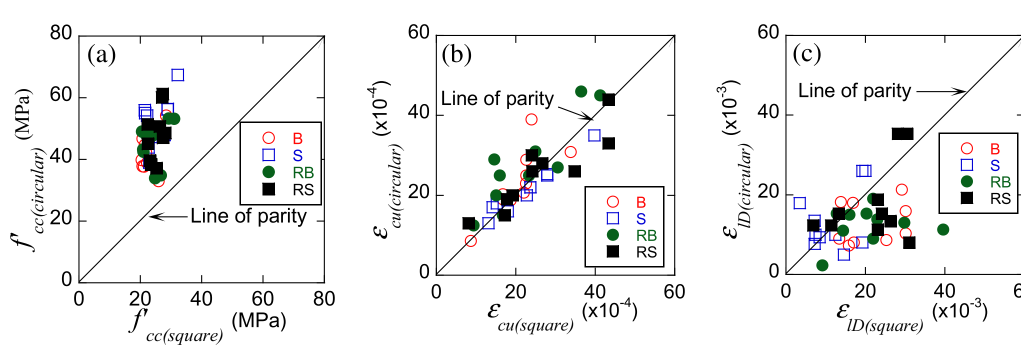

Fig. 11. Effects of specimen geometry/shape on axial capacity, axial strain, and lateral strain.

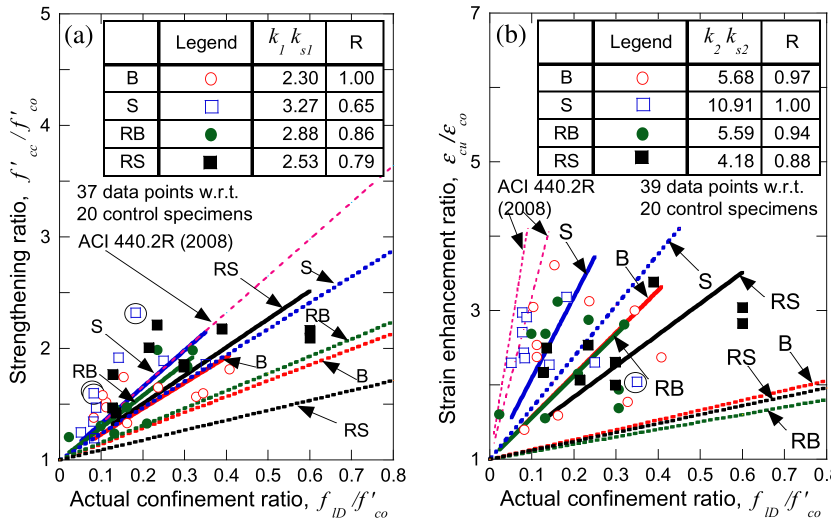

Fig. 12. Plots for estimating the confinement models' coefficients for circular columns in the ultimate state. (a) Strengthening ratio vs. actual confinement ratio plots for CFRP-confined and GFRP-confined columns. The ACI 440.2R [8] relationships are plotted for reference. (b) Strain enhancement ratio vs. actual confinement ratio plots for CFRP-confined and GFRP-confined columns. The ACI 440.2R [8] relationships for CFRP and GFRP confinement used in this study are also plotted for reference. The relationships for square columns are plotted using dotted lines (data from Islam et al. [9]).

terms of the Los Angeles abrasion values of the stone aggregates, as was also used in the current study. Furthermore, the Pearson's *R* values for the circular column data shown in the figures were found to be closer to unity than were the values associated with square columns. More similar *R* values for circular stone aggregate concrete columns relative to the values of square columns are reasonable based on the various effects at play for the cross section and geometry of square columns.

4. Conclusions

(a) Plain concrete columns composed of brick and recycled aggregates exhibiting greater dilation under axial compression than those composed of stone aggregates results in the following: (i) a significant increase in the initial stiffness indicating an early mobilization of FRP confinement in concretes having larger dilation properties and (ii) a marked decrease in the final stiffness in the stress–strain responses of such concrete columns. Initiation of the formation of microcracks in concretes having larger porosities (and hence more significant dilation properties) at a critical stress level that is lower than that for the stone aggregate concrete has been attributed to the first observation, whereas the existence of larger numbers of fracture planes compared to stone aggregate concrete has been attributed to the second observation.

(b) Due to the uniform stress distribution, the initial stiffness increase effect was more significant for circular columns than for square columns. The observed trend in the change in final stiffness values between significantly dilatable and less dilatable concretes for square columns suggests a delayed fracturing process of the side concrete after confinement is mobilized toward the four corners.

(c) High-definition video and still images demonstrate that rapid post-peak failure events occurred in confined columns experiencing either large dilation or larger confining pressures. This pattern requires future design attention to ensure the appropriate safety factors for the relevant cases.

(d) The relationships between the strengthening and strain enhancement ratios and the actual confinement ratio were plotted to measure the confinement effectiveness coefficients and the strain enhancement coefficients for the ultimate state for circular columns for concretes composed of each of the coarse aggregate types. In contrast to the observations for the square concrete columns, the measured coefficients in the circular columns were found to be similar for all aggregate types. This result strongly confirms that uniformity in the confining pressure distribution is favorable for harnessing similar confinement effectiveness for all aggregate types in the ultimate state. Therefore, for rectangular columns, the effects of dilation are predicted to be more severe in association with decreases in the confined concrete strength due to the greater nonuniformity of the confining pressure distribution of rectangular columns, even when compared to square columns.

Acknowledgments

The authors are grateful to the members and staff of the Concrete Laboratory and Structural Mechanics Laboratory, Department of Civil Engineering, Bangladesh University of Engineering and Technology, for their support and cooperation in conducting the tests. The authors gratefully acknowledge the kind cooperation extended by the LaMaCo System Sdn Bhd, Malaysia, in providing samples of the fiber-reinforced polymer wraps used in this investigation. The authors also sincerely acknowledge the funding provided by the Committee for Advanced Studies and Research, BUET, Dhaka, Bangladesh. The technical assistance provided by M/S Aziz & Company Limited, Dhaka, Bangladesh is also gratefully acknowledged.

Appendix A. Supplementary data

Supplementary data associated with this article can be found, in the online version, at http://dx.doi.org/10.1016/j.conbuildmat.2015.11.003.

References

[1] H. Saadatmanesh, M.R. Ehsani, M.W. Li, Strength and ductility of concrete columns externally reinforced with fiber composite straps, ACI Struct. J. 91 (4) (1994) 434–447.

[2] A. Mirmiran, M. Shahawy, Dilation characteristics of confined concrete, Mech. Cohes. Frictional Mater. 2 (3) (1997) 237–249.
[3] A. Mirmiran, M. Shahawy, Behavior of concrete columns confined by fiber composites, J. Struct. Eng. ASCE 123 (5) (1997) 583–590.
[4] M. Shahawy, A. Mirmiran, T. Beitelman, Tests and modeling of carbon-wrapped concrete columns, Compos. B Eng. 31 (6) (2000) 471–480.
[5] J.G. Teng, J.F. Chen, S.T. Smith, L. Lam, FRP: strengthened RC structures, Front. Phys. 1 (2002).
[6] L. Lam, J.G. Teng, Design-oriented stress–strain model for FRP-confined concrete in rectangular columns, J. Reinf. Plast. Compos. 22 (13) (2003) 1149–1186.
[7] L. Lam, J.G. Teng, Design-oriented stress–strain model for FRP-confined concrete, Constr. Build. Mater. 17 (6) (2003) 471–489.
[8] ACI-440, Guide for the design and construction of externally bonded FRP systems for strengthening concrete structures (ACI 440.2 R-08), ACI committee 440 American Concrete Institute Farmington Hills, Michigan, 2008.
[9] M.M. Islam, M.S.I. Choudhury, A.F.M.S. Amin, Dilation effects in FRP-confined square concrete columns using stone, brick, and recycled coarse aggregates, J. Compos. Constr. ASCE (2015), http://dx.doi.org/10.1061/(ASCE)CC.1943-5614.0000574. 04015017.
[10] A. Hasnat, M.M. Islam, A.F.M.S. Amin, Enhancing the debonding strain limit for CFRP-strengthened RC beams using U-clamps: identification of design parameters, J. Compos. Constr. ASCE (2015), http://dx.doi.org/10.1061/(ASCE)CC.1943-5614.0000599. 04015039.
[11] S.P. Shah, S. Chandra, Critical stress, volume change, and microcracking of concrete, ACI J. Proc. 65 (9) (1968) 770–780.
[12] Y.H. Loo, A new method for microcrack evaluation in concrete under compression, Mater. Struct. 25 (10) (1992) 573–578.
[13] A. Bascoul, State of the art report—Part 2: mechanical micro-cracking of concrete, Mater. Struct. 29 (2) (1996) 67–78.
[14] T. Akçaoğlu, M. Tokyay, T. Çelik, Assessing the ITZ microcracking via scanning electron microscope and its effect on the failure behavior of concrete, Cem. Concr. Res. 35 (2) (2005) 358–363.
[15] Y.B. Zaitsev, F.H. Wittmann, Simulation of crack propagation and failure of concrete, Materiaux et Constr. 14 (5) (1981) 357–365.
[16] R.L. Carrasquilio, A.H. Nilson, Microcracking and behavior of high strength concrete subject to short-term loading, ACI J. Proc. 78 (3) (1981) 179–186.
[17] R.S. Ravindrarajah, R.N. Swamy, Load effects on fracture of concrete, Mater. Struct. 22 (1) (1989) 15–22.
[18] J.C. Lim, T. Ozbakkaloglu, Stress–strain model for normal-and light-weight concretes under uniaxial and triaxial compression, Constr. Build. Mater. 71 (2014) 492–509.
[19] B. González-Fonteboa, F. Martínez-Abella, J. Eiras-López, S. Seara-Paz, Effect of recycled coarse aggregate on damage of recycled concrete, Mater. Struct. 44 (10) (2011) 1759–1771.
[20] A.A. Akhtaruzzaman, A. Hasnat, Properties of concrete using crushed brick as aggregate, Concr. Int. 5 (2) (1983) 58–63.
[21] T.U. Mohammed, A. Hasnat, M. Awal, S. Bosunia, Recycling of brick aggregate concrete as coarse aggregate, J. Mater. Civ. Eng. (2014), http://dx.doi.org/10.1061/(ASCE)MT.1943-5533.0001043. B4014005.
[22] A.F.M.S. Amin, A. Hasnat, A.H. Khan, M. Ashiquzzaman, Residual cementing property in recycled fines and coarse aggregates: occurrence and quantification, J. Mater. Civ. Eng. (2015), http://dx.doi.org/10.1061/(ASCE)MT.1943-5533.0001472 (In publication queue).
[23] J.C. Lim, T. Ozbakkaloglu, Confinement model for FRP-confined high-strength concrete, J. Compos. Constr. 18 (4) (2014). 04013058.
[24] T. Ozbakkaloglu, J.C. Lim, T. Vincent, FRP-confined concrete in circular sections: review and assessment of stress–strain models, Eng. Struct. 49 (2013) 1068–1088.
[25] T. Vincent, T. Ozbakkaloglu, Influence of concrete strength and confinement method on axial compressive behavior of FRP confined high-and ultra high-strength concrete, Compos. B Eng. 50 (2013) 413–428.
[26] T. Ozbakkaloglu, J.C. Lim, Axial compressive behavior of FRP-confined concrete: experimental test database and a new design-oriented model, Compos. B Eng. 55 (2013) 607–634.
[27] J.C. Lim, T. Ozbakkaloglu, Design model for FRP-confined normal-and high-strength concrete square and rectangular columns, Mag. Concr. Res. 66 (20) (2014) 1020–1035.
[28] Y. Xiao, H. Wu, Compressive behavior of concrete confined by carbon fiber composite jackets, J. Mater. Civ. Eng. ASCE 12 (2) (2000) 139–146.
[29] M.S.I. Choudhury, Confinement effect of fiber reinforced polymer wraps on circular and square concrete columns, Dept. of Civil Engineering, Bangladesh Univ. of Engineering and Technology 2012, Dhaka, Bangladesh, 2012 (M.Sc. thesis).
[30] M.M. Islam, Interaction diagrams for square concrete columns confined with fiber reinforced polymer wraps, Dept. of Civil Engineering, Bangladesh Univ. of Engineering and Technology 2011, Dhaka, Bangladesh, 2011 (M.Sc. thesis).
[31] K. Abdelrahman, R. El-Hacha, State-of-the-art Review on FRP Strengthened Concrete Columns, Taylor and Francis, London, Concrete Solutions, 2014, pp. 253–260.
[32] M.N. Youssef, M.Q. Feng, A.S. Mosallam, Stress–strain model for concrete confined by FRP composites, Compos. B Eng. 38 (5) (2007) 614–628.
[33] J. Teng, Y. Huang, L. Lam, L. Ye, Theoretical model for fiber-reinforced polymer-confined concrete, J. Compos. Constr. 11 (2007) 201–210.
[34] D. Sfer, I. Carol, R. Gettu, G. Etse, Study of the behavior of concrete under triaxial compression, J. Eng. Mech. 128 (2) (2002) 156–163.